INTERNATIONAL JOURNAL FOR NUMERICAL METHODS IN FLUIDS
Int. J. Numer. Meth. Fluids 2004; **44**:91–114 (DOI: 10.1002/fld.630)

A low-dimensional description of transient shear-thinning free-surface flow in thin cavities, as applied to injection molding

Sheng X. Zhang and Roger E. Khayat*,†

Department of Mechanical and Materials Engineering, The University of Western Ontario, London, Ont., Canada N6A 5B9

SUMMARY

A spectral methodology is proposed to examine the influence of shear thinning on the transient free-surface flow inside a three-dimensional thin cavity. The problem is closely related to the filling stage during the injection molding process. The moving domain is mapped onto a rectangular domain at each time step of the computation. A modified pressure is introduced that is governed by the Laplace's equation. The flow field is expanded in Fourier series along the lateral direction in the mapped domain, and the Galerkin projection is used to derive the equations that govern the expansion coefficients, which are solved using a variable-step finite-difference scheme. This approach is valid for simple and complex cavities as illustrated for the cases of a flat plate with variable and constant thickness. It is shown that, even for highly non-linear shear-thinning flow, only a few modes are needed for convergence. Shear thinning generally influences the flow behaviour. However, shear thinning may enhance or prohibit the flow, depending whether the flow rate at the entrance of the cavity is fast or slow, respectively.

1. INTRODUCTION

Transient free-surface flows belong to the important class of moving-boundary problems, which remain challenging because of the non-linearities involved. This is particularly true for non-Newtonian flow. Even for Newtonian flow, the prescription of contact conditions between moving boundary and solid wall, the implementation of kinematic and dynamic conditions at the moving boundary, the estimation of curvature in the presence of surface tension, and the discretization of a moving domain, are just some of the many difficult issues encountered in the simulation of free surface and multiphase flows. These difficulties are considerably amplified for three-dimensional problems. Typically, a boundary-value problem of the moving

*Correspondence to: R. E. Khayat, Department of Mechanical and Materials Engineering, The University of Western Ontario, London, Ont., Canada N6A 5B9.
†E-mail: rkhayat@eng.uwo.ca

Contract/grant sponsor: Natural Sciences and Engineering Research Council of Canada

Received 15 July 2002
Revised 19 June 2003

type involves geometric and material non-linearities that must be addressed as well as an unknown boundary, a free surface or an interface. In contrast to conventional problems in fluid dynamics, the domain of computation, which is bounded in part by the free surface, is not known *a priori* since the shape of the free surface itself must be determined as part of the solution. For steady-state flow, such as the flow at the exit of a die, a number of iterations are usually needed in order to reach the precise form of the free surface. In this case, domain discretization is not a major difficulty [1]. The problem becomes even more challenging when, in addition, the shape of the free surface evolves with time, generating large distortions in the discretized domain of the fluid. While large distortions have been reasonably well handled for two-dimensional free-surface flows, major issues remain open regarding complex three-dimensional problems.

Several numerical techniques have been developed for the solution of moving boundary/initial value problems. These techniques may be classified as Eulerian, Lagrangian and mixed Eulerian–Lagrangian [2, 3]. In the Eulerian description of the flow, the grid points remain stationary or move in a predetermined manner [4–7]. Typically, the fluid moves in and out of the computational cells. The method can handle arbitrarily large free-surface deformations without loss of accuracy. Its main disadvantage, however, is the lack of sharp definition of the free surface, and the consequent difficulty to impose the kinematic and dynamic boundary conditions on the free surface. In the Lagrangian approach, the grid points move with local fluid particles [8, 9]. The free surface is sharply defined and it is easy to impose the necessary boundary conditions. However, Lagrangian methods require mesh refinement or remeshing for large deformation of the free surface. Hybrid methods have also been developed that combine the advantages of the Eulerian and Lagrangian methods [10]. Most methods dealing with the simulation of the filling of injection molding are based on the Hele–Shaw or thin-shell assumption, which ignores the variation of the flow in the thickness direction [11–14]. These studies have been essentially based on the finite-element method (FEM), and therefore are limited because of the frequent remeshing requirement under transient and non-linear conditions.

Khayat and co-workers extended the shallow-water or lubrication formulation to cover non-linear problems such as high-speed lubrication problems, and thin-film coating flow of Newtonian at high inertia [15–17] and non-Newtonian flows [18, 19]. The lubrication formulation reduces the problem by one dimension as a result of the dominant horizontal scale(s) over the depthwise direction, z. In other words, given the large horizontal length scales relative to the depth, the variation of the velocity across the film becomes negligible, particularly in the diffusive terms, where shear effects are assumed to dominate elongation effects. Consequently, the pressure reduces to its hydrostatic part; it varies only with gravity in the vertical direction. Various models can be incorporated, to cover both laminar and turbulent flows, for any geometry. Two different approaches are usually adopted in the literature, the most common of which is based on the long-wave approximation, which neglects the depthwise flow component entirely, and the other method accounts for the vertical flow similarly to boundary-layer theory. A major problem is encountered, however, by both methods, since the dependence of the flow on the depth must be explicitly given in order to reduce the problem. If, on the one hand, fluid inertia is neglected, as in slow lubrication problems, the approximation of the velocity does not pose any problem since the x and y momentum equations are readily integrable in the z direction. If, on the other hand, inertia is present, then the z dependence of the velocity must be approximated in order to integrate the convective terms in the mo-

mentum equations. Various approximations have been used in the literature, but, predominantly, a semi-parabolic profile in z is used for laminar flow, and a flat (plug-flow) profile is used for turbulent flow. These approximations, however, are not valid under conditions of strong non-linearities, such as high inertia, or strong shear and elongation flows. Khayat and co-workers proposed an effective spectral representation of the velocity profile in terms of z was implemented, coupled with a Galerkin projection technique, which provided excellent agreement with the Watson's similarity solution in the limit of steady two-dimensional liquid spreading [15].

These recent studies by Khayat and co-workers were, however, limited to planar or axisymmetric flows. Similar spectral methodologies will be used in the present work that lead to a low-dimensional spectral description of the three-dimensional transient free-surface flow for a shear-thinning fluid. The problem is challenging since, on the one hand, conventional domain methods are inadequate for adaptive meshing, and, on the other hand, integral methods such as the boundary-element method, which can handle more easily adaptive meshing, are less effective for non-linear flow. In the present paper, the difficulties with conventional methods are circumvented by devising a hybrid Lagrangian/Eulerian method, which consists of mapping the irregular moving domain, at each time step, onto a fixed rectangular domain. In order to handle the highly non-linear effects in the averaged equation in the horizontal plane, the spectral method is used. The flow field is expanded in Fourier series in the transverse direction, and the finite-difference method is used to obtain the expansion coefficients. The method is used to obtain the three-dimensional flow field inside a thin cavity. This corresponds to the solution of a large class of free-surface flow problems, with close relevance to polymer processing. The flow is typically encountered during the filling stage inside a thin cavity as in injection molding. The lubrication assumption is adopted to derive the resultant equations for a shear-thinning fluid, averaged over the thickness of the cavity.

2. GENERAL FORMULATION

In this section, the basic assumptions for the lubrication formulation are first briefly reviewed for viscous shear-thinning fluids. The theory is then extended to include the transient free-surface flow inside thin three-dimensional cavities.

2.1. General lubrication theory and flow domain

Consider an incompressible inelastic non-Newtonian fluid of density ρ, and viscosity μ. Surface tension effect is assumed to be negligible. If (x_1, x_2, x_3) denotes the three-dimensional system of Cartesian co-ordinates, then the conservation equations for an incompressible fluid can be concisely written as

$$u_{j,j} = 0, \quad \rho(u_{i,T} + u_j u_{i,j}) = -P_{,i} + \lfloor \mu(u_{i,j} + u_{j,i}) \rfloor_{,j} \tag{1}$$

where $i, j = 1, 2, 3$, u_i are the velocity components, P is the hydrostatic pressure, and T is the time. The summation convention is assumed, and a subscript after a coma denotes partial differentiation. In this work, the fluid is assumed to obey the power law for

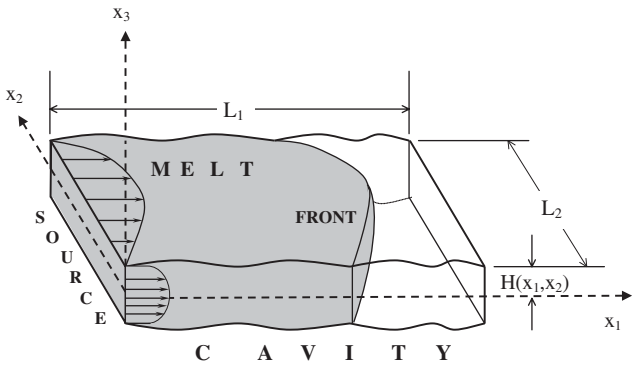

Figure 1. Schematic illustrating the transient free-surface flow inside a cavity induced by the imposed flow at the source boundary, Γ_s.

viscosity [20]:

$$\mu(\dot{\Gamma}) = m_0 \,|\, \dot{\Gamma}|^{n-1} \tag{2}$$

where m_0 is a material constant, n is the power-law exponent, and $\dot{\Gamma}$ is the square root of the second invariant of the rate-of-strain tensor.

The lubrication assumption is the hydrodynamic analogue of shell theory. In most lubrication films the thickness of the film is small compared with the lateral dimensions, or with the local radius of curvature. Properly handled, this assumption can be used to eliminate the dependence upon one of the three spatial variables from the hydrodynamic equations and boundary conditions. The continuity equation is integrated across the film and the conservation equations are used to evaluate the quantities appearing as integrands. Consider the free-surface flow of a thin continuous film of incompressible fluid between two rigid surfaces as shown schematically in Figure 1. For simplicity, the flow is assumed to be symmetric with respect to the (x_1, x_2) plane, so that $x_3 \in [-H(x_1,x_2), +H(x_1,x_2)]$, where $2H(x_1,x_2)$ is the thickness of the plate.

In lubrication theory, the conservation equations (1) are formulated in the narrow-gap limit [12]. It is convenient to cast these equations in terms of dimensionless variables. Typically, in three-dimensional thin-cavity flow, there are three characteristic lengths, L_1 and L_2 along the lateral directions x_1 and x_2, and H_0, representing the thickness of the cavity in the x_3 direction. Note that, typically, $H_0 \ll L_1, L_2$. Figure 1 shows a step of the filling stage of a thin cavity of general shape. If L_1 and L_2 are of the same order, L_0, then the dimensionless variables may be introduced as follows:

$$\begin{aligned} (x, y) &= \frac{1}{L_0}(x_1, x_2), \quad z = \frac{x_3}{H_0}, \quad t = \frac{V_0}{L_0} T, \quad h = \frac{H}{H_0} \\ (u_x, u_y) &= \frac{1}{V_0}(u_1, u_2), \quad u_z = \frac{u_3}{V_0 \varepsilon}, \quad p = \varepsilon^2 \frac{L_0}{\mu_0 V_0} P, \quad \eta = \frac{\mu}{\mu_0} \end{aligned} \tag{3}$$

where V_0 is a typical (reference) velocity, $\mu_0 = m_0 (V_0/L_0)^{1-n}$, and $\varepsilon = H_0/L_0$ is the aspect ratio.

Upon carrying out the change of variables and excluding terms of $O(\varepsilon)^2$, the dimensionless continuity and momentum conservation equations reduce to

$$u_{\alpha,\alpha} + u_{z,z} = 0 \tag{4}$$

$$\varepsilon^2 \,\mathrm{Re}(u_{\alpha,t} + u_j u_{\alpha,j}) = -p_{,\alpha} + (\eta u_{\alpha,z})_{,z} \tag{5}$$

$$p_{,z} = 0 \tag{6}$$

where a Greek Index corresponds to x and y, and a Latin Index corresponds to x, y and z. The dimensionless viscosity is explicitly given by

$$\eta(\mathbf{r},t) = |u_{\alpha,z}\, u_{\alpha,z}|^{(n-1)/2} = |z|^{(n-1)/n} |\nabla p(\mathbf{x},t)|^{(n-1)/n} \tag{7}$$

Here $\mathbf{r}(x,y,z)$ is the position vector of a point in space, and $\mathbf{x}(x,y)$ is its projection vector in the (x,y) plane. If the continuity equation is integrated between $z=0$ and $z=h$, and inertia effect is neglected in the momentum equation, then the following equation for the pressure is obtained [12, 21]:

$$(h(\mathbf{x})^{(2n+1)/n} |\nabla p(\mathbf{x},t)|^{(1-n)/n} p_{,\alpha}(\mathbf{x},t))_{,\alpha} = 0 \tag{8}$$

Dependence on time of the pressure in the equation above is of course implicit since the flow is assumed to be quasi-steady as a result of neglecting inertia.

2.2. *Boundary and initial conditions*

Regarding the boundary conditions, the lubrication formulation does not accommodate adherence conditions at the lateral walls, at $x_2 = 0$ and $x_2 = L_2$ (for straight lateral walls). Stick boundary conditions can only be applied at the bottom and upper surfaces, $x_3 = +H$ and $x_3 = -H$, respectively (see Figure 1). This assumption is not as unrealistic as it seems, since the flow core in a thin cavity is not significantly affected by the boundary-layer region at the lateral walls. In this case, only the no-penetration condition applies along the lateral walls. The flow is assumed to be driven by an imposed (dimensionless) pressure gradient, $q_0(y,z,t)$, at $x=0$, so that the general boundary condition at the entrance to the cavity is given by

$$q(x=0,y,z,t) = q_0(y,z,t) \tag{9}$$

where $q(\mathbf{r},t) = \mathbf{n}(\mathbf{r},t) \cdot \nabla p(\mathbf{r},t)$ is the directional derivative of the pressure along the normal direction, and $\mathbf{n}$ is the normal vector. The pressure gradient may be either maintained fixed at all time, or adjusted according to the flow conditions inside the cavity (mold). A time-dependent pressure gradient corresponds typically to the inlet condition in injection molding where the pressure rather than the flow rate is varied with time at the source of fluid. Although a variable pressure gradient at the entrance to the cavity can be easily accommodated by the present formulation, q_0 will be assumed to depend only on y. Since the lubrication assumption can only accommodate the no-penetration conditions

$$\mathbf{n}(\mathbf{r},t) \cdot \nabla p(\mathbf{r},t) = 0 \tag{10}$$

is assumed to hold at the lateral walls.

At the front (free surface) the imposition of a suitable dynamic condition is not obvious for thin-cavity flow. It is clear that for the general three-dimensional flow, and in the absence of surface tension effect, a zero-traction condition must apply at the front. If the front is represented by $x = X(y,z,t)$ for $z \in [-h,h]$, and $t > 0$, and $\mathbf{n}(y,z,t)$ is the unit normal vector to the front, then it can be shown that, to leading order, the dynamic condition at $x = X(y,z,t)$ becomes [21]

$$p(x = X, y, z, t) = 0 \tag{11}$$

Finally, the kinematic condition at the free surface is the least obvious among the boundary conditions to implement. In a Lagrangian representation, the moving boundary is assumed to deform with the fluid velocity, such that the evolution of free surface is governed by the equation

$$\frac{\mathrm{d}\mathbf{r}}{\mathrm{d}t} = \mathbf{u}(\mathbf{r}, t) \tag{12}$$

where $\mathbf{r}$ and $\mathbf{u}$ is the position and velocity vectors at the front. Although easy to implement, the resulting scheme based on Equation (12) tends to sweep points on the moving boundary along the tangent to the moving boundary, even if only small shape changes take place. Consequently, frequent redistribution of the moving boundary points or remeshing would be necessary if relation (12) is used. Alternatively, the moving boundary can be assumed to deform pointwise along the normal with the normal projection of the fluid velocity at the moving boundary [2]. This method keeps the points evenly distributed on the moving boundary. The alternative kinematic boundary condition is obtained by taking the scalar product of Equation (12) with the vector $\mathbf{n}$, and noting that $\mathbf{n} \cdot \mathbf{n} = 1$, one has $\mathbf{n} \cdot (\mathrm{d}\mathbf{r}/\mathrm{d}t) = \mathbf{n} \cdot \mathbf{n}(\mathbf{n} \cdot \mathbf{u})$. An equivalent solution of this equation leads to an alternative kinematic condition [2]. In this case, the free surface deforms only in the normal direction. Although this condition requires the calculation of the normal vector at the free surface, no remeshing of the free-surface points is needed in this case since the points remain evenly distributed on the free surface. Moreover, the condition is particularly advantageous to use in the present context. This advantage will become evident when the solution of the pressure equation is carried out in the (x, y) plane. However, Equation (12) can be more advantageous because of simplicity of implementation. In the current study, the difficulty with node sweeping will be easily circumvented once an Eulerian form of (12) is adopted (see below).

As to the initial conditions, the fluid is assumed to be initially at rest, occupying a finite non-zero domain, which will be specified later.

3. SOLUTION PROCEDURE

The solution of Equation (8) is now obtained subject to the appropriate boundary conditions on the cavity wall and free surface. The flow domain in the horizontal plane is first mapped onto a rectangular domain. The solution of the mapped equation is obtained by using the method of Galerkin projection. This method consists of expanding the pressure in Fourier series. The expansion coefficients are then determined by solving the projected equations. However, the problem is considerably simplified after Equation (8) is reduced to an equivalent Laplace's equation.

3.1. Domain of computation and reduced problem

The domain of computation is obviously the projection $\Omega_{xy}(t)$ of the physical domain $\Omega(t)$ onto the (x, y) plane. Equation (8) has an equivalent Laplace's equation if the following quantity, $S(\mathbf{x}, t)$, is introduced such that

$$S_{,\alpha}(\mathbf{x}, t) = h(\mathbf{x})^{(2n+1)/n} |\nabla p(\mathbf{x}, t)|^{(1-n)/n} p_{,\alpha}(\mathbf{x}, t) \tag{13}$$

In this case, S must satisfy the Laplace's equation

$$S_{,xx}(\mathbf{x}, t) + S_{,yy}(\mathbf{x}, t) = 0 \tag{14}$$

The corresponding boundary conditions for Equation (14) are obtained from conditions (9)–(12). For simplicity, the cavity is assumed to be straight at the entrance, with $x = 0$ and $y \in [-1, +1]$, and the flow is assumed to enter the cavity at a flow rate that depends only on y. Thus, at the entrance to the cavity, $q_0(y, t) = p_{,x}$ $(x = 0, y, t)$, and condition (9) reduces to

$$S_{,x}(x = 0, y, t) = -h^{(2n+1)/n}(x = 0, y) |q_0(y, t)|^{(1-n)/n} q_0(y, t) \tag{15}$$

At the lateral walls, Equation (10) yields

$$\mathbf{n}(\mathbf{x}) \cdot \nabla S(\mathbf{x}, t) = 0 \tag{16}$$

Finally, at the front, the dynamic condition (11) asserts that $\mathrm{d}p(x = X, y, t)$ along the free surface (curve in the horizontal plane) or $\mathrm{d}p = p_{,x}\,\mathrm{d}x + p_{,y}\,\mathrm{d}y = 0$. Upon multiplying this equation by $h^{(2n+1)/n}|\nabla p|^{(1-n)/n}$, one obtains that $\mathrm{d}S = 0$ along the front. One can then set

$$S(x = X, y, t) = 0 \tag{17}$$

Once $S(\mathbf{x}, t)$ is determined from Equation (14), at a given time, t, the velocity components are then obtained, which are given by

$$u_\alpha(\mathbf{r}, t) = \left(\frac{n}{n+1}\right) \frac{1}{h(\mathbf{x})} \left[1 - \left(\frac{z}{h(\mathbf{x})}\right)^{(n+1)/n}\right] S_{,\alpha}(\mathbf{x}, t) \tag{18a}$$

$$u_z(\mathbf{r}, t) = \left(\frac{n}{n+1}\right) \frac{h_{,\alpha}(\mathbf{x})}{h^2(\mathbf{x})} z \left[1 - \left(\frac{z}{h(\mathbf{x})}\right)^{(n+1)/n}\right] S_{,\alpha}(\mathbf{x}, t) \tag{18b}$$

Equation (12) is used to determine the evolution of the front in three-dimensional space, which is rewritten here as

$$U_x(y, z, t) = X_{,t}(y, z, t) + U_y(y, z, t) X_{,y}(y, z, t) + U_z(y, z, t) X_{,z}(y, z, t) \tag{19}$$

where $U_i(y, z, t) = u_i(x = X, y, z, t)$, $i = x, y, z$, are the velocity components at the front.

3.2. Domain mapping

In order to represent the modified pressure, S, in series of orthonormal functions, the domain of computation must be rectangular. For this, the physical domain $(x, y) \in \Omega_{xy}(t)$ is mapped onto the domain $(\xi, \zeta) \in [0, 1] \times [-1, 1]$. The mapping is schematically shown in Figure 2. More specifically, consider the projection of the flow, at a given time, in the (x, y) plane. If the width

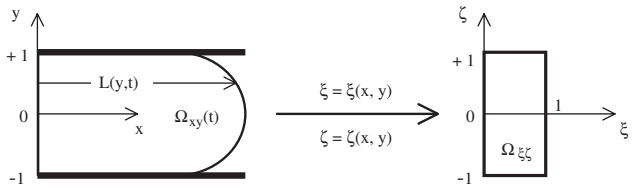

Figure 2. Mapping of the middle slice of the time-dependent physical domain in the (x, y) plane onto the rectangular computational domain in the (ξ, ζ) plane.

at $x = 0$ is taken as twice the reference length, L_0, then $\Omega_{xy}(t) = \{(x, y) | x \in [0, X], y \in [-1, 1]\}$. In this case, let the mapping be given by

$$\tau(x, y, t) = t, \quad \xi(x, y, t) = \frac{x}{L(y, t)}, \quad \zeta(x, y, t) = y \tag{20}$$

where $L(y, t) = X(y, z = 0, t)$. Upon use of expressions (20), Equation (14) for the modified pressure reads

$$[1 + (\xi L_{,\zeta})^2] S_{,\xi\xi} + [2\xi (L_{,\zeta})^2 - \xi L L_{,\zeta\zeta}] S_{,\xi} - 2 L L_{,\zeta} S_{,\xi\zeta} + L^2 S_{,\zeta} = 0 \tag{21}$$

subject to the following boundary conditions:

$$S_{,\xi}(\xi = 0, \zeta, \tau) = a^2 |\zeta^2 - 1|^{(1-n)/n} (\zeta^2 - 1) \tag{22a}$$

where a is a positive quantity, reflecting the strength of the incoming flow

$$S(\xi = 1, \zeta, \tau) = 0 \tag{22b}$$

$$S_{,\zeta}(\xi, \zeta = -1, \tau) = 0 \tag{22c}$$

$$S_{,\zeta}(\xi, \zeta = +1, \tau) = 0 \tag{22d}$$

Note that S is coupled to the shape of the front, $X(y, z, t)$, which must be determined as part of the solution, thus making the problem non-linear. The shape of the front in turn delimits the domain in the (x, y) plane. Once $S(x, y, t)$ is obtained at a given time, the horizontal velocity components at the front are evaluated. $X(y, z, t)$ is then determined by solving the kinematic equation (19), which, in the horizontal plane, reduces to

$$U(y, t) = L_{,t}(y, t) + V(y, t) L_{,y}(y, t) \tag{23}$$

where $U(y, t) = U_x(y, \mathbf{z} = 0, t)$, and $V(y, t) = U_y(y, z = 0, t)$.

3.3. Pressure expansion

Since the flow is assumed to be symmetric with respect to the y-axis, the modified pressure can be expressed as

$$S(\xi, \zeta, \tau) = \sum_{n=0}^{\infty} S_n(\xi, \tau) \cos n\pi\zeta \tag{24}$$

Note that expression (24) satisfies the two lateral boundary condition (22c) and (22d). Obviously, a truncation level will have to be imposed, leading to a finite number of modes, M, in the expansion. If expression (24) is substituted into Equation (21), and the Galerkin projection method is used, then the following recursive relation is obtained for the pressure coefficients:

$$\sum_{n=0}^{M} A_{mn} S_{n,\xi\xi} + \sum_{n=0}^{M} B_{mn} S_{n,\xi} + \sum_{n=0}^{M} C_{mn} S_n = 0 \tag{25}$$

where the time-dependent coefficient matrices are given by

$$\begin{aligned} A_{mn}(\xi,\tau) &= \int_{-1}^{+1} \cos(m\pi\zeta)\cos(n\pi\zeta)[1+(\xi L_{,\zeta})^2]\,\mathrm{d}\zeta \\ B_{mn}(\xi,\tau) &= \int_{-1}^{+1} \cos(m\pi\zeta)\{[2\xi(L_{,\zeta})^2 - \xi XX_{,\zeta\zeta}]\cos(n\pi\zeta) + 2n\pi LL_{,\zeta}\sin(n\pi\zeta)\}\,\mathrm{d}\zeta \\ C_{mn}(\xi,\tau) &= n^2\pi^2 \int_{-1}^{+1} L^2\cos(n\pi\zeta)\cos(m\pi\zeta)\,\mathrm{d}\zeta \end{aligned} \tag{26}$$

In this case, the Galerkin projection consists of multiplying Equation (21) by $\cos(m\pi\zeta)$ for $m \in [1, M]$, and integrating it with respect to ζ from -1 to 1, after substituting expression (24). The resulting system (25) can be regarded as a set of ordinary differential equations (since time τ appears only implicitly) with $2M$ degrees of freedom.

Once system (25) is solved, $S(\mathbf{x}, t)$ is determined over the domain $\Omega_{xy}(t)$, in particular along the boundary $\Gamma_{xy}(t)$, the horizontal components of the velocity at the front are determined from Equation (18a) by setting $z = 0$, leading to

$$U(y,t) = \left(\frac{n}{n+1}\right)\frac{1}{h(L)}\,S_{,x}(L,y,t) \tag{27a}$$

$$V(y,t) = \left(\frac{n}{n+1}\right)\frac{1}{h(L)}\,S_{,y}(L,y,t) \tag{27b}$$

Similarly to the pressure expansion (24), $L(y,t)$ is expanded as

$$L(y,t) = \sum_{n=0}^{M} L_n(t)\cos n\pi y \tag{28}$$

The Galerkin projection is used to solve Equation (23), and the coefficients $L_n(t)$ are governed by following set of coupled ODEs:

$$\frac{\mathrm{d}L_n(t)}{\mathrm{d}t} = \sum_{n=0}^{M} D_{mn}(t)L_n(t) + E_m(t) \tag{29}$$

where the coefficients are given by

$$\begin{aligned} D_{mn}(t) &= n\pi \int_{-1}^{+1} \cos(m\pi y)\sin(n\pi y)V(y,t)\,\mathrm{d}y \\ E_m(t) &= \int_{-1}^{+1} \cos(m\pi y)U(y,t)\,\mathrm{d}y \end{aligned} \tag{30}$$

Systems (25) and (29) are solved simultaneously as a set of algebraic-differential equations involving $3M$ degrees of freedom. An explicit backward-finite-difference scheme in time is used to solve system (29), which then determines the front position within an error of less than 1 per cent. System (25) is solved using a variable-step finite-difference scheme in space. The basic discretization is the trapezoidal rule over a non-uniform mesh. This mesh is chosen adaptively, to make the local error approximately the same size everywhere. Higher-order discretizations are obtained by differed corrections and global error estimates are produced to control the computation. The linear system of equations is solved using a special form of Gauss elimination that preserves sparseness. The tolerance is generally kept lower than 10^{-6}.

4. NUMERICAL RESULTS

The formulation and solution procedure are now used to examine the transient free-surface flow inside thin cavities. The flow field is first examined for a highly shear-thinning fluid ($n=0.2$). The influence of the number of modes, M, is assessed for this highly non-linear flow. The influence of shear thinning on the cavity flow is then examined in some detail. Finally, the influence of cavity thickness is investigated for both Newtonian and shear-thinning flows. All results are given in terms of dimensionless quantities. The initial domain occupied by the fluid in the (x, y) plane is taken to correspond to $\Omega_{xy}(t=0)=\{(x,y)|x\in[0,\frac{1}{2}+\frac{1}{2}(y^2-1)^2], y\in[-1,1]\}$. The flow rate is imposed by prescribing $p_{,x}$ at $x=0$. In this work, $p_{,x}(x=0,y,t)=a(y-1)(y+1)$, where a is a constant to be specified later.

4.1. Flow of a highly shear-thinning fluid and numerical assessment

Consider the flow of a shear-thinning fluid inside a flat cavity of constant thickness. The Power-law Index is $n=0.2$. The length and the width are taken along the x and y directions, respectively, with the x-axis lying half-way between the lateral sides of the cavity (see Figure 2). In this problem, $a=2$. Although the fluid is flowing predominantly in the x direction, there is a strong secondary flow in the y direction as well. Figure 3 shows the evolution of the front in the (x, y) plane between the two lateral flat walls at $y=\pm 1$. The front is shown

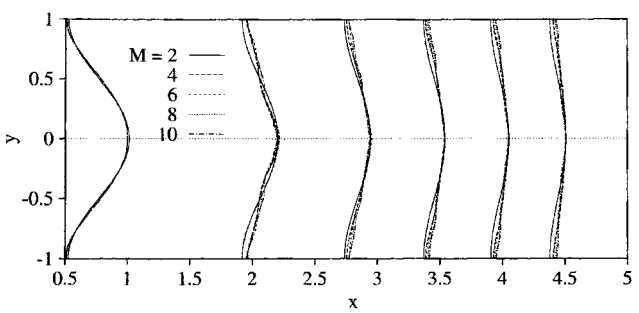

Figure 3. Influence of the number of modes on the transient flow of a shear-thinning fluid ($n=0.2, a=2$) inside a flat plate. The fronts are shown at equal time intervals over a period of 5 time units, for $M\in[2,10]$. The arrows in this and subsequent figures indicate the direction with time.

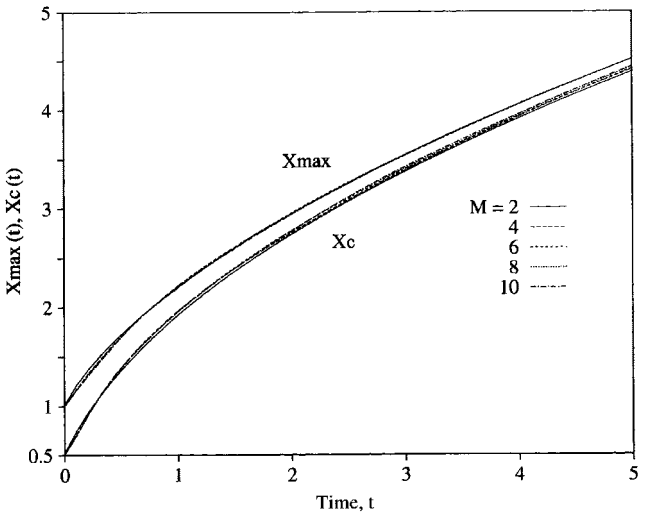

Figure 4. Influence of the number of modes on the evolution of the front tip position, $X_{\max}(t)$, and that of contact, $X_c(t)$, with time for the flow inside a flat plate of Figure 3.

at equal intervals over a period of 5 time units. Note that the initial domain is shown partially for clarity since it extends to $x=0$. The calculations are carried out for different levels of truncation, corresponding to $M \in [2, 10]$. The figure clearly shows the fast rate of convergence, despite the presence of strong non-linearities. This is confirmed below.

The sequence of flow fronts in Figure 3 shows a relatively dominant axial flow at the lateral walls ($y=\pm 1$), which leads to the straightening of the front with time. Indeed, the fluid in the vicinity of the lateral boundaries tends to flow faster than that at the front tip (due to slippage), eventually straightening the front. The figure indicates that the front becomes essentially straight after some time, despite the parabolic driving pressure gradient at the entrance $x=0$. It is interesting to observe that the maximum flow at $x=0$ does not induce a relatively strong maximum in the middle of the front. The spacing between two successive fronts diminishes with time, which is of course expected since a time-independent pressure gradient is imposed at the entrance, whose effect weakens as additional flow enters the cavity.

A better quantitative assessment of convergence and accuracy is achieved by monitoring the time evolution of the front tip, $X_{\max}(t)$, and that the contact point, $X_c(t)$. Figure 4 displays the evolution of $X_{\max}$ and X_c for the same truncation levels, $M \in [2, 10]$. The starting point, at $t=0$, is $X_{\max}(0)=1$ and $X_c(0)=0.5$, corresponding to the initial fluid domain. Although $X_{\max}$ and X_c increase monotonically with time, the rate of increase drops continuously with time. The influence of higher-order modes is insignificant in this case. In fact, the use of only two modes leads to a reasonably accurate result. Convergence is clearly attained for $M \geqslant 2$. The results for $M > 2$ are essentially the same, confirming the observations based on Figure 3. Table I shows the numerical values for X_c and $X_{\max}$ at $t=5$, together with the difference between two successive values. Convergence is shown to be oscillatory. Figure 4 and Table I indicate that the two-mode solution tends to slightly underestimate the value of X_c in general, and slightly overestimate the $X_{\max}$ value for $t<0.5$. Additional calculations show

Table I. Influence of number of modes and convergence assessment for shear-thinning fluid ($n=0.2$, $a=2$) inside a flat plate. The table shows the position values of the contact and tip points at $t=5$.

M	X_c $(t=5)$	Δ	$X_{max}(t=5)$	Δ
2	4.37844	0.00000	4.50548	0.0000
4	4.40406	0.02056	4.50646	0.00098
6	4.40952	0.00546	4.50422	−0.00224
8	4.42531	0.0157	4.50773	0.00351
10	4.43325	0.00794	4.50713	−0.00060

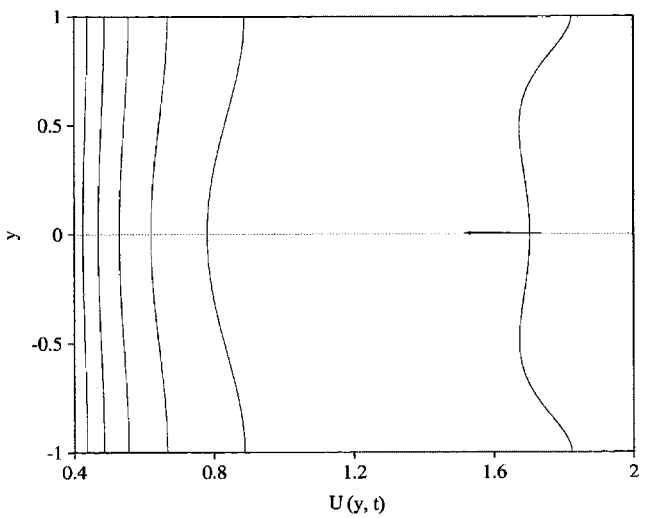

Figure 5. Evolution of the distribution of the axial velocity component, $U(y,t)$, at the front for $0<t<5$, for the flow in Figure 3. The arrows in this and subsequent figures indicate the direction in time.

that the rate of convergence is generally high for a flow with a different initial domain, or a flow in curved cavities. Although the results for $M>2$ are slightly more accurate, the results below are reported for $M=2$ for clarity. Recall that the current convergence assessment is based on the highly non-linear flow with $n=0.2$. The inclusion of higher-order modes leads to increasing modulation (with M), which makes the evolution of the velocity components, especially in phase space, difficult to interpret. It is emphasized that the inclusion of a few higher-order modes does not even increase noticeably the CPU time for the computation.

The strength of the lateral flow is further appreciated by examining the horizontal velocity components at the front. Figures 5 and 6 show the distributions of the axial and lateral velocity components at the front, $U(y,t)$ and $V(y,t)$, respectively. The profiles are shown over a period of 5 time units, corresponding to the flow in Figure 3. The arrow in the figures indicates the time direction. The discrepancy between the velocity of the front tip, $U(0,t)$, and that of the points of contact, $U(\pm 1,t)$, is obvious from Figure 5, particularly in the initial stages. The discrepancy decreases with time. It is interesting to observe from the figure that, initially, the minimum axial flow occurs roughly half-way between the lateral wall and the middle

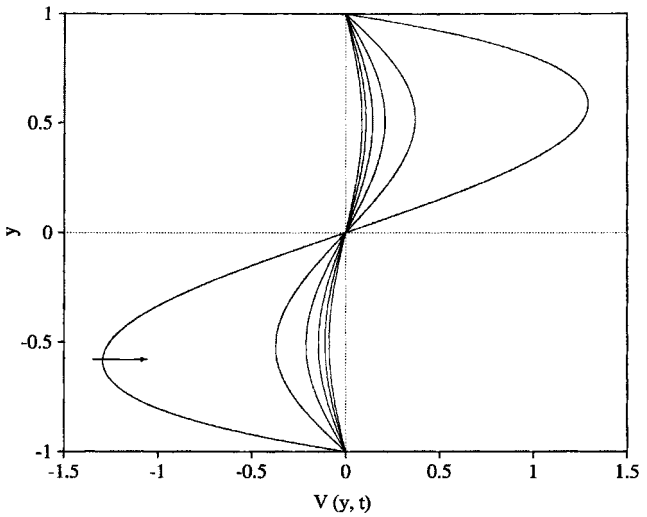

Figure 6. Evolution of the distribution of the lateral velocity component, $V(y,t)$, at the front for $0<t<5$, for the flow in Figure 3.

($y=\pm 0.5$). Eventually the minimum occurs at $y=0$. The figure also shows that the velocity tends to generally converge in the long time everywhere, including near the lateral walls. The axial flow decreases considerably, more than 4 times its initial value over 5 time units. The lateral velocity component, $V(y,t)$, is strongest initially, and is generally of the same order of magnitude as $U(y,t)$, as depicted from Figure 6. As expected, the lateral velocity vanishes at $y=\pm 1$. However, there is a sharp drop in $V(y,t)$ near the lateral boundaries. This drop becomes weaker with time. It is also interesting to observe from Figure 6 that $V(y,t)$ is highly non-linear initially, and is essentially linear near the middle ($y=0$) as time increases. The overall non-linear behaviour is further assessed in Figure 7, which shows the phase plot in the (U,V) plane. The phase plots are closed orbits that are similar to those emerging from dynamical systems. They tend to decrease in the overall diameter, confirming the weakening of the flow with time. The width of the orbit represents the difference between $U(0,t)$ and $U(\pm 1,t)$.

4.2. Influence of shear thinning on transient behaviour

The influence of shear thinning is now investigated on the front evolution and corresponding flow field. The level of shear thinning is of course imposed through the value of the power-law exponent n. It will be seen shortly that n is not the only factor that influences the departure from Newtonian behaviour. One expects shear thinning to relatively accelerate the flow, but this is not always the case. There is a strong interplay between the level of shear thinning and the magnitude of the driving pressure. Shear-thinning level is varied over the range $n\in[0.2,1]$, where it is recalled that $n=1$ corresponds to a Newtonian fluid. Two levels of driving pressures at $x=0$ will be considered, corresponding to $a=1$ and 2.

Consider first the case of a relatively high driving pressure ($a=2$). The resulting flow is represented in Figure 8, which shows the evolution of the free surface for $n=1$, 0.6

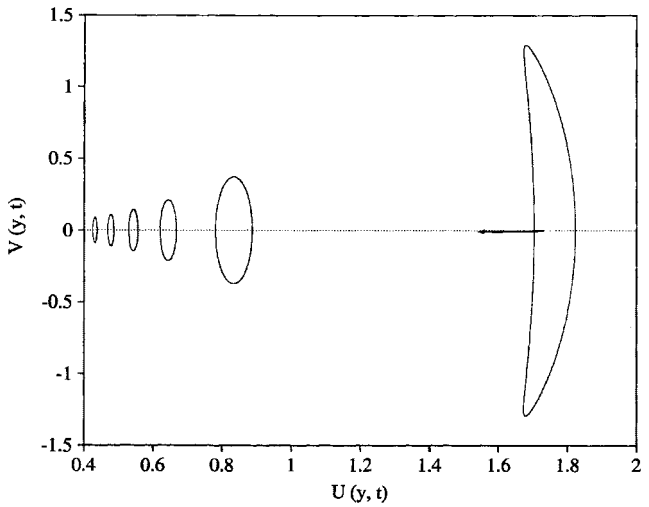

Figure 7. Phase plot of the axial and lateral velocity components, $U(y,t)$ and $V(y,t)$, at the front for $0<t<10$, for the flow in Figure 3.

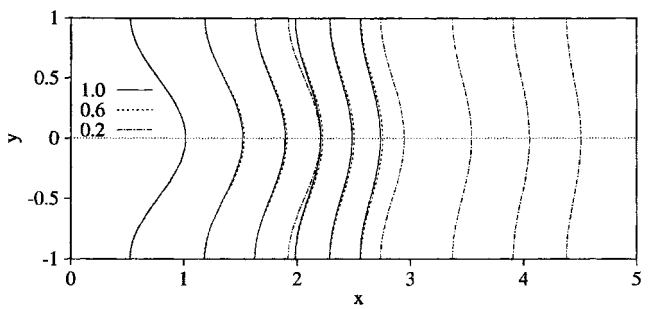

Figure 8. Influence of shear thinning on transient flow inside a flat plate of constant thickness ($a=2$). The fronts are shown at equal time intervals over a period of 5 time units, for $n=0.2$, 0.6 and 1.0.

and 0.2. It is observed that a shear-thinning fluid penetrates the cavity faster than a Newtonian. What is even more interesting to observe from the figure is the substantial drop in rate of penetration as n decreases from 0.6 to 0.2. The increase in rate (as n decreases) is far from being linear with n since the flows at $n=1$ and 0.6 advance at essentially the same rate. The non-linear influence of shear thinning is further quantified by examining $X_{\max}(t)$ and $X_c(t)$, which are depicted from Figures 9 and 10. Both figures show that the flow response (at least in the middle and lateral walls) is essentially Newtonian for $n>0.5$. It is important to observe, in addition to the actual values of $X_{\max}$ and X_c, the rate of increase of these two quantities, which is much higher for a shear-thinning fluid ($n>0.5$). This is also confirmed by examining the evolution of the horizontal velocity components at the front, which can be summarized by the phase plot in the (U,V) plane as shown in Figure 11. The figure shows only two cases, $n=0.2$ and 1.0, for clarity.

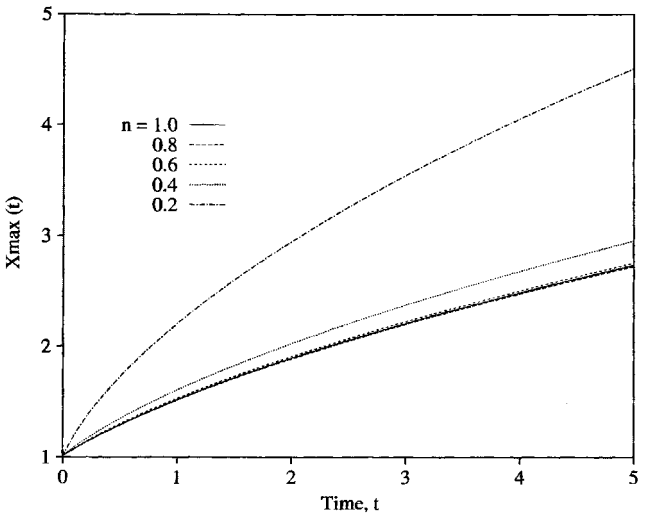

Figure 9. Influence of shear thinning on the evolution of the front tip position, $X_{\max}(t)$, with time for the flow inside a flat plate of constant for $n \in [0.2, 1.0]$ $(a = 2)$.

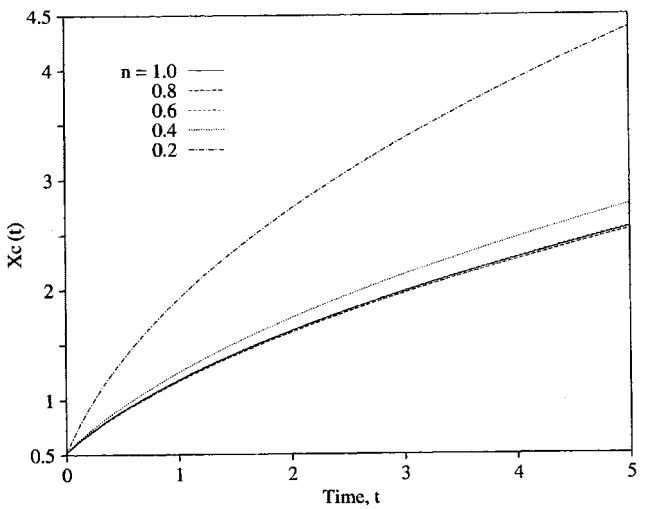

Figure 10. Influence of shear thinning on the evolution of the front contact point position, $X_c(t)$, with time for the flow inside a flat plate of constant for $n \in [0.2, 1.0]$ $(a = 2)$.

As mentioned above, there is an important interplay between shear thinning and the flow rate. The results in Figures 8–11 indicate that shear thinning tends to enhance the flow. This is in fact what one would expect since viscous effects are effectively reduced in the presence of shear thinning. However, in Hele–Shaw flow, there is a slip at the wall, which tends to enhance fluid movement and reduce the overall shear rate. For a constant thickness,

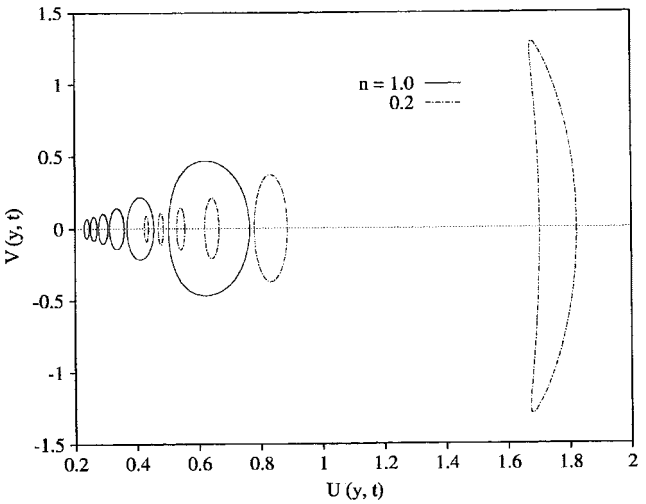

Figure 11. Phase plot of the axial and lateral velocity components, $U(y,t)$ and $V(y,t)$, at the front for $0<t<5$, for the flow in Figure 8. The plots are shown only for $n=0.2$ and 1.0 for clarity.

expression (12a) indicates that the horizontal velocity components are given by

$$U(y,t) = -\left(\frac{n}{n+1}\right) p_{,x}(\mathbf{x},t)|\nabla p(\mathbf{x},t)|^{(1-n)/n} \tag{31a}$$

$$V(y,t) = -\left(\frac{n}{n+1}\right) p_{,y}(\mathbf{x},t)|\nabla p(\mathbf{x},t)|^{(1-n)/n} \tag{31b}$$

Expressions (31) illustrate the interplay between shear thinning and the flow rate, which is implicitly related to the pressure gradient. The relation between the Newtonian and non-Newtonian velocities can be roughly written as $(U,V)_{\text{non-Newt}} = 2(n/n+1)|\nabla p|^{(1-n)/n}(U,V)_{\text{Newt}}$. Thus, shear-thinning flow is stronger than a Newtonian flow if the product $2(n/n+1)|\nabla p|^{(1-n)/n)} > 1$, or if the pressure gradient is strong enough to counterbalance the decrease in the term $n/(n+1)$ as n decreases from 1. Note that, for shear-thinning fluids, this term is less than one.

Figure 12 shows the influence of shear thinning on the evolution of the front for a flow rate corresponding to $a=1$, for $n=1.0$, 0.6 and 0.2. The flow in the figure should be compared to that of Figure 8 where the flow rate is twice as strong ($a=2$). Contrary to Figure 8, Figure 12 indicates that the flow of a shear-thinning fluid is slower than that of a Newtonian fluid. Figure 12 also shows that the acceleration is much smaller in this case. This is confirmed upon examination of $X_{\max}(t)$, which is shown in Figure 13 for $n \in [0.2, 1.0]$. There is a strong tendency for the tip position to evolve linearly with time, especially for the more shear-thinning fluids. It is important to observe from the figure that, unlike the case $a=2$ (Figure 9), the effect of shear thinning is gradual (linear) on the flow. The overall weakening of the flow with shear thinning is illustrated in Figure 14 for $n=0.2$, 0.4 and 1.0. There is considerable weakening of both horizontal velocity components with shear thinning (compare with Figure 11). In particular, the fluid corresponding to $n=0.2$ remains essentially stationary, similarly to what

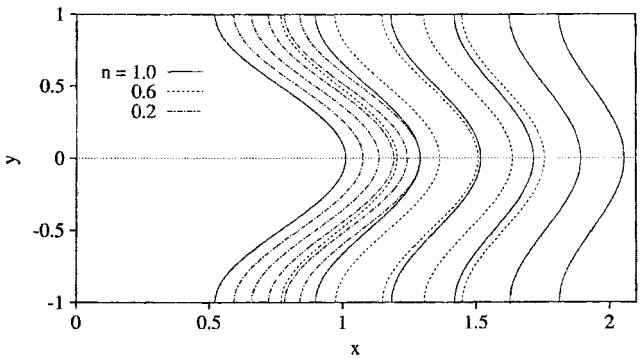

Figure 12. Influence of shear thinning on transient flow inside a flat plate of constant thickness ($a = 1$). The fronts are shown at equal time intervals over a period of 5 time units, for $n = 0.2$, 0.6 and 1.0.

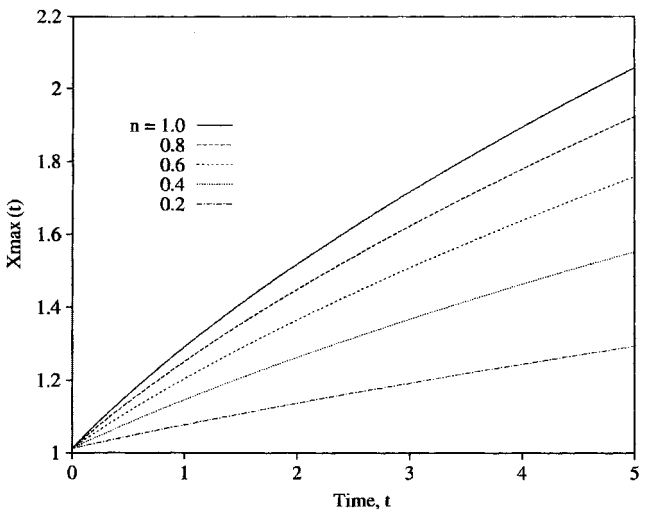

Figure 13. Influence of shear thinning on the evolution of the front tip position, $X_{\max}(t)$, with time for the flow inside a flat plate of constant thickness for $n \in [0.2, 1.0]$ and $a = 1$.

Figure 12 seems to suggest. This observation is important from a practical standpoint, as it suggests that shear thinning can be considerably inhibiting to fluid movement in a given process such as injection molding.

Finally, the results in Figures 9, 10, and 13 hint at the existence of a flow rate at which shear thinning may not have any influence on the flow. Indeed, Figure 15 shows the evolution of $X_{\max}$ and X_c for $n = 0.2$ and 0.8, for a flow rate corresponding to $a = 1.5$. The figure clearly reflects the insignificance of the influence of n on the flow, comparatively to a flow at higher flow rate, $a = 2$ (Figures 9 and 10), and a flow at lower rate, $a = 1$ (Figure 13). It is interesting to note from Figure 15 that shear thinning appears to enhance slightly the movement of the tip of the front, and appears to retard slightly the movement of the contact point.

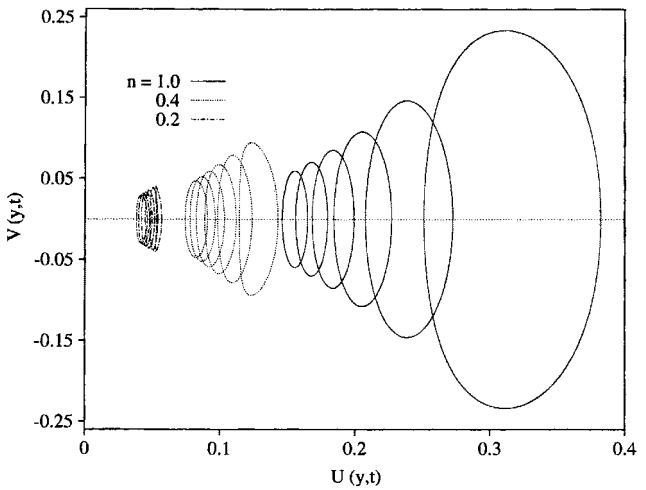

Figure 14. Phase plot of the axial and lateral velocity components, $U(y,t)$ and $V(y,t)$, at the front for $0<t<5$, for the flow in Figure 12 ($a=1$). The plots are shown only for $n=0.2$, 0.4 and 1.0 for clarity.

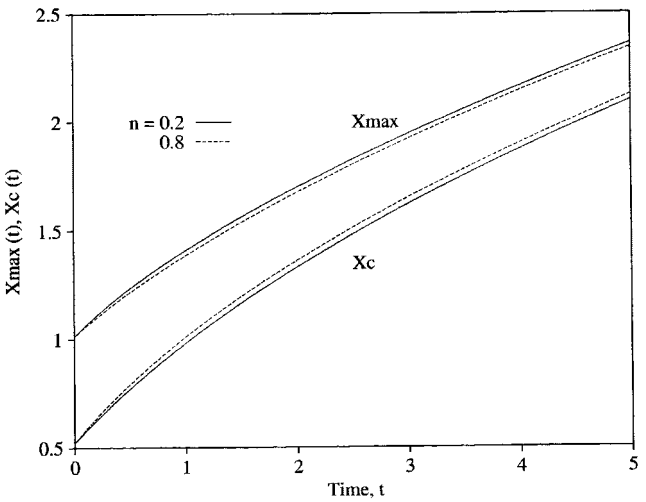

Figure 15. Influence of shear thinning on the evolution of the front tip position, $X_{\max}(t)$, and that of the contact point position, $X_c(t)$, with time for the flow inside a flat plate of constant thickness for $n \in [0.2, 1.0]$ and $a=1.5$.

4.3. *Influence of cavity thickness*

So far, all reported results have been restricted to a cavity of constant thickness, $h(\mathbf{x})=1$. In this section, the influence of cavity thickness is examined for the flow of shear-thinning fluids. Similarly to the interplay between shear thinning and flow rate, it is expected that an

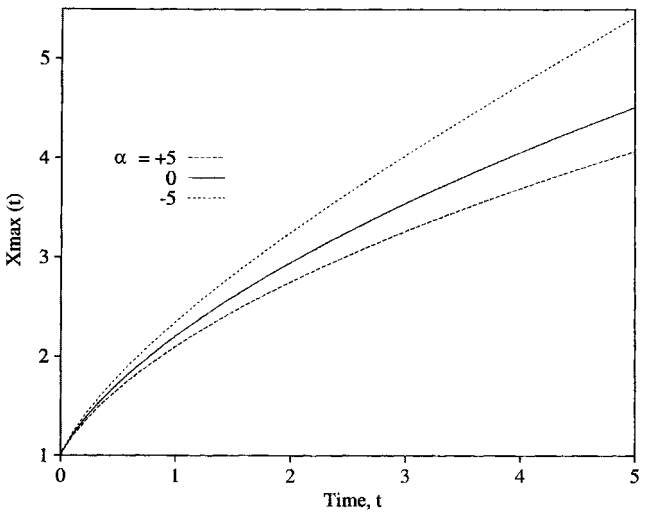

Figure 16. Influence of cavity surface inclination on the evolution of the front tip position, $X_{\max}(t)$, for $n=0.2$ and $a=2$. Here α is the angle of inclination (in degrees).

interplay can exist with cavity thickness. However, the influence of cavity thickness may be more intricate given its local character, as opposed to the global influence of the flow rate at the entrance. Three types of thickness distributions will be investigated, a linearly diverging, linearly converging and wavy cavity. Only variation along the x direction will be examined.

Consider first the flow inside a cavity of thickness $h(\mathbf{x})=\tan(\alpha)x+1$, where α is the angle of inclination of the cavity walls. The influence of α on the flow is illustrated in Figure 16 for three values: $\alpha=+5$, 0 and -5°, corresponding to a diverging, flat and converging cavity, respectively. The flow rate is the same for the three configurations, corresponding to $a=2$, and $n=0.2$. As expected, the figure shows that the flow is weakened by cavity expansion ($\alpha=+5^\circ$). More explicitly, Figure 17 gives the relative strength of the lateral flow. The figure indicates, in particular, that the difference in flow strength between the middle ($y=0$) and the lateral walls ($y=\pm 1$) tends to increase for with cavity expansion.

Finally, consider the flow inside a cavity with wavy walls. In this case, the thickness is taken as $h(\mathbf{x})=1+A\sin(\omega x)$, where A is the amplitude and ω is frequency. Figure 18 shows the influence of $A\in[0,0.8]$ on the evolution of the front tip position, $X_{\max}(t)$, for a shear-thinning fluid ($n=0.2$), $\omega=4$ and $a=2$. Case $A=0$ corresponds to a cavity of constant thickness, and is included here for references. The figure shows that as A is increased from zero, the flow behaves in an oscillatory manner with time. There does not seem to be a fixed frequency in the flow response, but the flow appears to fluctuate mostly in the initial stage. Initially, the period of flow is roughly equal to 1.5 time unit, corresponding to a flow frequency equal to 4.2. Thus, the flow responds with the same time frequency as the imposed space frequency of the wall. This is expected, since the mean velocity at the channel exit is equal to one. It is interesting to observe that the frequency of the flow is not affected by the amplitude A. The effect of wall frequency is further assessed in Figure 19, which shows the influence of $\omega\in[0,4]$ on $X_{\max}(t)$ for a shear-thinning fluid ($n=0.2$), $A=0.8$ and $a=2$. Generally, the front

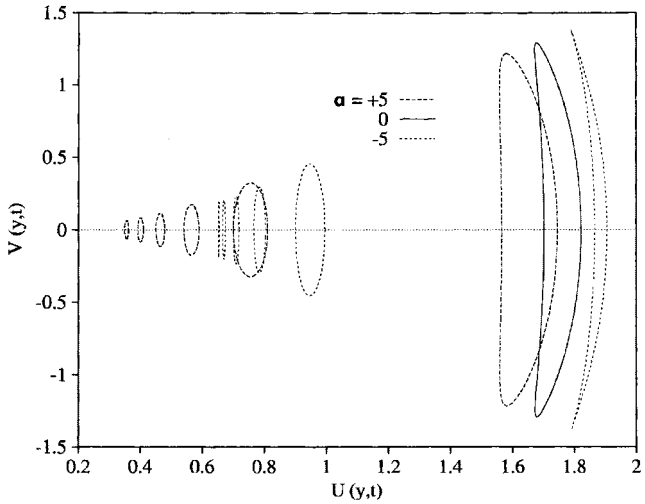

Figure 17. Phase plot of the axial and lateral velocity components, $U(y,t)$ and $V(y,t)$, at the front for $0<t<5$, for the flows corresponding to Figure 15. Note that only the initial orbit is shown for the Newtonian case.

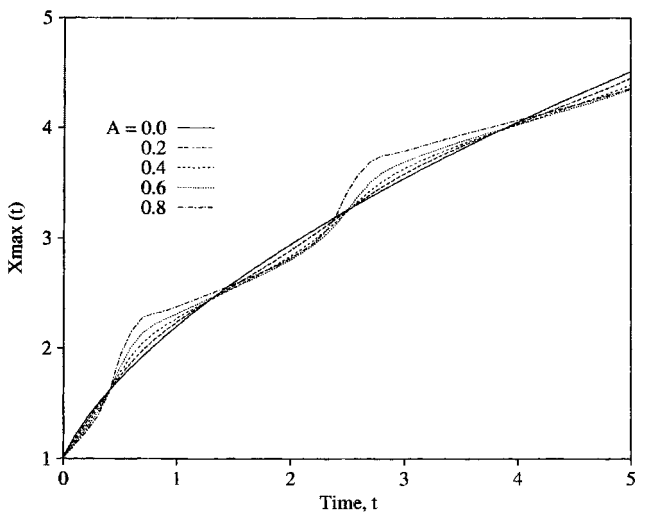

Figure 18. Influence of thickness amplitude, A, on the evolution of the front tip position, $X_{\max}(t)$, for wavy cavity wall, $\omega=4$, $n=0.2$ and $a=2$.

tip moves at the same average rate as for a flow between flat walls. However, there is a sharp drop in rate as ω is increased from zero to 1, and a gradual regain in the value of $X_{\max}(t)$ as ω increases further. The response amplitude of the flow is affected by ω. For low ω, the amplitude is relatively large. Figure 20 shows influence of shear thinning, $n\in[0.2,1.0]$, on the flow response for $A=0.8$, $\omega=4$, and $a=2$. The results in the figure should be compared

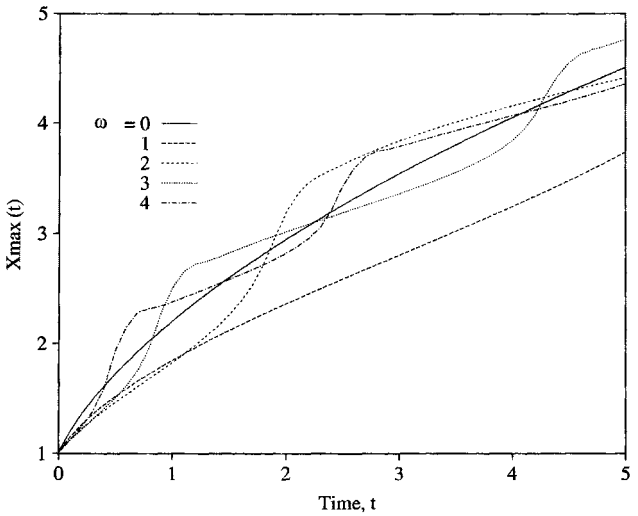

Figure 19. Influence of thickness frequency, ω, on the evolution of the front tip position, $X_{\max}(t)$, for wavy cavity wall, $A = 0.8$, $n = 0.2$ and $a = 2$.

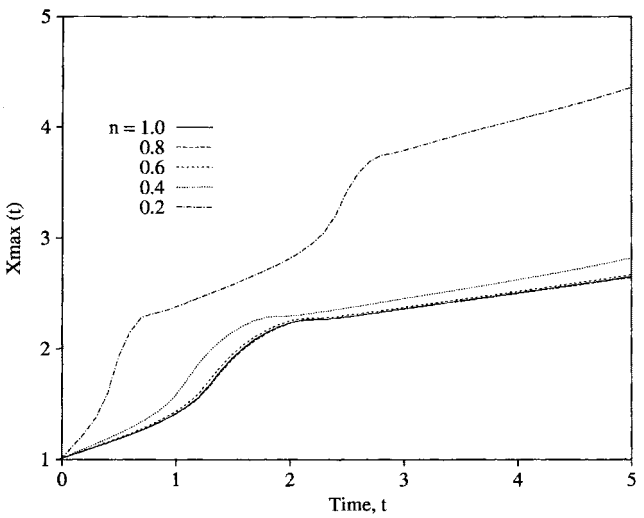

Figure 20. Influence of shear thinning on the evolution of the front tip position, $X_{\max}(t)$, for wavy cavity wall, $A = 0.8$, $\omega = 4$ and $a = 2$.

to those reported in Figure 9. Similarly to a flat cavity, the flow in the present case is also little influenced by shear thinning for $n > 0.2$. The important observation to be made from Figure 20 is that the response frequency is independent of shear thinning for $n > 0.2$. As n is decreased to 0.2, the response frequency roughly doubles.

5. DISCUSSION AND CONCLUSION

A number of assumptions were made in this work, which need to be relaxed if a more realistic model is sought to simulate the filling stage during injection molding. These assumptions include fluid incompressibility, inelasticity, absence of inertia and surface tension, isothermal laminar flow, small gap width compared with other dimensions, rapid variation of mold shape (large local radius of curvature), and no slippage at the mold walls. The absence of surface tension and fluid elasticity can be particularly limiting. Although polymeric fluids have typically low surface tension coefficient, there may be instances where surface tension effect becomes important, such as in the presence of strong local curvature of the front in the (x, y) plane. The presence of insert, for instance, can lead to significant curvature in the melt front as the fluid wraps itself around the insert. Surface tension effect is also important at the contact between front and mold wall. It is, however, well established that polymeric fluids have a low surface-tension coefficient (small capillary number), and unless the flow is very slow, surface-tension effect is not expected to play a significant role in injection molding.

The effect of fluid elasticity is another important aspect that needs eventually to be incorporated. Elastic effect becomes clearly non-negligible in flow regions where normal-stress or elongation effect is strong. Since the flow is expected, typically, to be reasonably fully developed in most of the flow regions behind the front, then elasticity is relatively weak in those regions, particularly as far as the flow kinematics is concerned. A rough estimate of the flow elongation in the front region for a shear-thinning fluid indicates elongation increases in strength for fluids that are highly shear thinning, flowing at a higher injection rate, in a mold of smaller gap width [22]. Elastic effect can also be important in the final stages of filling. Elasticity should then be considered when estimating stress buildup and residual stresses. This estimation is of course relevant to the prediction of warpage and shrinkage of the molded part. In addition to elongation, shearing can also enhance elastic effect in the flow, in the form of shear-rate dependence of the relaxation time(s), for instance. However, shearing is expected to be almost negligible, particularly in the immediate vicinity of the mold walls and in the central region, but may exhibit some strength further away from the walls. In this regard, the adoption of an appropriate constitutive model that can accommodate both shear and elongation effects becomes a crucial and difficult issue to deal with if elastic effects are included. Comparison between theory and experiment shows that flow simulation based on inelastic fluids can be realistic. This has even been established based on earlier studies on injection molding. Huang [23] has used the marker-and-cell approach to investigate the melt front flow. Assuming isothermal Newtonian and power-law fluid behaviour, he obtained fountain-flow patterns. His results are in good agreement with the experimental observations of Schmidt [24].

In conclusion, the general lubrication or shallow-water formulation is revisited for transient free-surface flow inside a three-dimensional cavity of variable thickness. The fluid is assumed to be shear thinning of the power-law type. A semi-analytical approach is used to solve the moving-boundary problem. Inertia is neglected, and a modified pressure, S, is introduced, which is governed by the Laplace's equation. The irregular and time-dependent domain in the (x, y) plane is mapped onto the fixed rectangular domain $(\xi, \zeta) \in [0, 1] \times [-1, 1]$. The transformed (modified) pressure equation is solved by expanding S in Fourier series along the ζ direction. A similar expansion is used to represent the shape of the front. The Galerkin projection method is used to obtain the equations that govern the expansion coefficients using a

multiple-step finite-difference method. Convergence and accuracy of the method are assessed by varying the level of truncation in the Fourier expansion. It is found that, even for the most non-linear case ($n = 0.2$), only a remarkably small number of modes are usually needed to reach convergence. This observation is consistent for the free-surface profiles, the advancement of front tip and contact point, and the distribution of the velocity components along the front.

The influence of shear thinning, and the cavity topography is examined in some detail. In all cases reported, the driving pressure gradient is parabolic with respect to the transverse direction, y, and is maintained fixed at the cavity entrance ($x = 0$). The initial domain is also assumed to have a parabolic front. There is a strong lateral flow initially. This flow, however, diminishes in intensity, leading to the straightening of the front with time. At high flow rate, shear thinning is found to enhance flow movement. When the flow rate is relatively low, shear thinning appears to prohibit the flow. Hence, there is a critical flow rate for which (even the strongest) shear-thinning effect ($n = 0.2$) does not alter the Newtonian flow. Variation in cavity topography indicates that a spatial modulation of the cavity surface(s) leads to temporal modulation of the flow. Shear thinning appears to enhance modulation.

ACKNOWLEDGEMENT

The present work is supported by the Natural Sciences and Engineering Research Council of Canada.

REFERENCES

1. Tanner RI. *Engineering Rheology*. Oxford, 1985.
2. Floryan JM, Rasmussen H. Numerical methods for viscous flows with moving boundaries. *Applied Mechanical Review* 1989; **42**:323.
3. Wang HP, Lee HS. Free and moving boundary value problems. In *Fundamentals of Computer Modeling for Polymer Processing*, Tucker III CL (ed.). Hanser: Munich, 1989.
4. Nickell RE, Tanner RI, Caswell B. The solution of viscous incompressible jet and free-surface flows using finite element method. *Journal of Fluid Mechanics* 1974; **65**:189.
5. Silliman WJ, Scriven LE. Separating flow near a static contact line: slip at a wall and shape of a free surface. *Journal of Computational Physics* 1980; **34**:287.
6. Ruschak KJ. A method of incorporating free boundaries with surface tension in finite element fluid flow simulation. *International Journal for Numerical Methods in Engineering* 1980; **15**:639.
7. Kawahara M, Miwa T. Finite element analysis of wave motion. *International Journal for Numerical Methods in Engineering* 1984; **20**:1193.
8. Bach P, Hassager O. An algorithm for the use of the Lagrangian specification in Newtonian fluid mechanics and applications to free surface flows. *Journal of Fluid Mechanics* 1985; **152**:173.
9. Ramaswany B, Kawahara M. Lagrangian finite element analysis applied to viscous free surface fluid flow. *International Journal for Numerical Methods in Fluids* 1987; **7**:953.
10. Chipada S, Jue TC, Joo SW, Wheeler MF, Ramaswamy R. Numerical simulation of free-boundary problems. *Computers and Fluid Dynamics* 1996; **7**:91.
11. Tadmor Z, Broyer E, Gutfinger C. Flow analysis network (FAN)—a method for solving flow problems in polymer processing. *Polymers Engineering and Science* 1974; **14**:660.
12. Hieber CA, Shen SF. A finite-element/finite-difference simulation of the injection molding process. *Journal of Non-Newtonian Fluid Mechanics* 1980; **7**:1.
13. Wang VH, Hieber CA, Wang KK. Mold filling simulation in injection molding of three-dimensional thin parts. *SPE Antec Tech papers* 1986; **32**:97.
14. Osswald TA, Tucker III CL. Compression mold filling simulation for non-planar parts. *International Polymer Processing* 1990; **5**:79.
15. Khayat RE, Welke S. Influence of inertia, gravity and substrate topography on the transient coating flow of a thin fluid film. *Physics of Fluids* 2001; **13**:355.
16. Siddique MR, Khayat RE. Influence of inertia and topography in thin cavity flow. *Physics of Fluids* 2002; **14**:1703.

17. Khayat RE. Influence of inertia on the transient axisymmetric free-surface flow inside thin cavities of arbitrary shape. *Physics of Fluids* 2001; **13**:3636.
18. Khayat RE. Transient two-dimensional coating flow of a viscoelastic fluid film on a substrate of arbitrary shape. *Journal of Non-Newtonian Fluid Mechanics* 2001; **95**:199.
19. Khayat RE. Transient free-surface flow inside thin cavities of viscoelastic fluids. *Journal of Non-Newtonian Fluid Mechanics* 2000; **91**:15.
20. Bird RB, Armstrong RC, Hassager O. *Dynamics of Polymeric Liquids* (2nd edn.), vol. 1. Wiley: New York, 1987.
21. Sheng S. A low-dimensional description of transient Newtonian and non-Newtonian free-surface flows in thin cavities. *Master of Engineering Science Thesis*, The University of Western Ontario, July, 2000.
22. Tadmor Z, Gogos CG. *Priniciples of Polymer Processing*. Wiley: New York, 1979.
23. Huang CF. Ph.D. Dissertation, Department of Chemical Engineering, Stevens Institute of Technology, Hobokeon, NJ, 1978.
24. Schmidt LR. A special mold and tracer technique for studying shear and exensional flows in a mold cavity during injection molding. *Polymer Engineering Science* 1974; **14**:797.

